HOKKAIDO UNIVERSITY

Title	Energy Budget Observations in the Central Canadian Arctic
Author(s)	ASUMA, Yoshio; MATSUKAWA, Yoshiki; KIKUCHI, Katsuhiro et al.
Citation	Journal of the Faculty of Science, Hokkaido University. Series 7, Geophysics, 11(1), 27-49
Issue Date	1998-03-20
Doc URL	https://hdl.handle.net/2115/8822
Type	departmental bulletin paper
File Information	11(1)_p27-49.pdf

Hokkaido University Collection of Scholarly and Academic Papers : HUSCAP

Jour. Fac. Sci., Hokkaido Univ., Ser. VII (Geophysics), Vol. 11, No. 1, 27-49, 1998.

Energy Budget Observations in the Central Canadian Arctic

Yoshio Asuma, Yoshiki Matsukawa, Katsuhiko Kikuchi

Division of Earth and Planetary Sciences, Graduate School of Science, Hokkaido University, Sapporo 060-0810, Japan

Kazuhisa Tsuboki and Ryuji Kimura

Ocean Research Institute, University of Tokyo, Tokyo 164-0014, Japan

(Received November 30, 1997)

Abstract

To examine the formation process of cold air masses, energy budget observations were carried out in the central Canadian Arctic during mid-winter 1994. A series of cold air mass formations under clear sky, under cloud and during blizzard conditions were observed during this period. Typical energy amounts in these various weather conditions are summarized. The cold air was produced near the surface and accumulated in a strong surface inversion layer as a ridge passed. When a trough approached, the winds became stronger, cold air was mixed upward and transported downstream and may have contributed to anticyclogenesis.

1. Introduction

It is well known that the Canadian Arctic is one of the strong cold air mass producing regions in the northern hemisphere, along with Siberia. From a global point of view, the polar regions are a heat sink and the lower latitudes are a heat source. The atmosphere in the troposphere plays an important role in the transportation of heat to keep the balance. Therefore, a better understanding of the cold air mass formation process in the Arctic region is useful for understanding the global weather system, the global climate change problem and interactions between high and mid-latitudes.

Oort (1974) estimated the energy balance of the Arctic atmosphere north of latitude 60°N using a radiosonde data set. He estimated that, averaged over the year, about 75% of radiative cooling energy in the polar cap is transported by atmospheric processes southward across 60°N. The remaining 25% of this energy is used up by the direct exchange of sensible and latent heat at the earth's

surface. The major part of the energy flux is transported in the lower atmosphere under 850 hPa in height. The transient and stationary eddy disturbances contribute more to the polarward energy exchange than the mean meridional circulation. Nakamura and Oort (1988) also estimated the energy budget in the polar regions north of 70°N using satellite radiation data, radiosonde data and statistics generated by the GCM model. They reported almost the same numbers for the energy budget of the winter north polar cap. About 2/3 of the radiative cooling energy is transported from the mid-latitude across 70°N in latitude and 1/3 is consumed as the sensible and latent heat at the surface. They also suggested the importance of transient and stationary disturbances for the energy transportation to the north polar cap.

As insolation does not reach the Arctic during winter polar night, radiative cooling predominates during the winter season. Therefore, qualitatively speaking, a strong cold air mass is produced during the Arctic winter. Bodurtha (1952) and Colucci and Davenport (1987) concluded from the climatological data set that rapid surface anticyclogenesis occurs over northwestern North America and southeastern Canada. Cold type anticyclones usually develop in northwestern North America downstream of amplifying 500 hPa ridges and mostly following 500 hPa trough amplification and cold air outbreaks over the east coast of North America. Relatively warm type anticyclones often intensify in southeastern Canada upstream of a moving 500 hPa trough and downstream of the 500 hPa cutoff low. The former type of anticyclogenesis is associated with the transformation of a maritime polar air mass into a continental polar air mass. This transformation process was numerically investigated by Curry (1983, 1987). She stressed that the radiative cooling of ice crystals and water droplets in the cold air mass play an important role in the transformation. This suggestion is consistent with the relationship between winter pressure systems and ice fog in Fairbanks, Alaska reported by Bowling et al. (1968). The latter type of anticyclogenesis has been reported by many investigators as being associated with cold air outbreaks on the east coast of North America (Dallavalle and Bosart, 1975; Colucci and Davenport, 1987; Konrad and Colucci, 1989; Tan and Curry, 1993; King et al., 1995; Konrad, 1996). They found other important forcing mechanisms for intensification to be cold air advection and anticyclonic vorticity advection. Adiabatic warming by descent associated with the intensifying anticyclone reduces the cooling effect. Anticyclonic vorticity mostly advects from the west associated with the upper trough. But the question to be investigated here is; where and how is the cold air produced?

Figure 1 shows the mean temperature and mean wind at 850 hPa in January

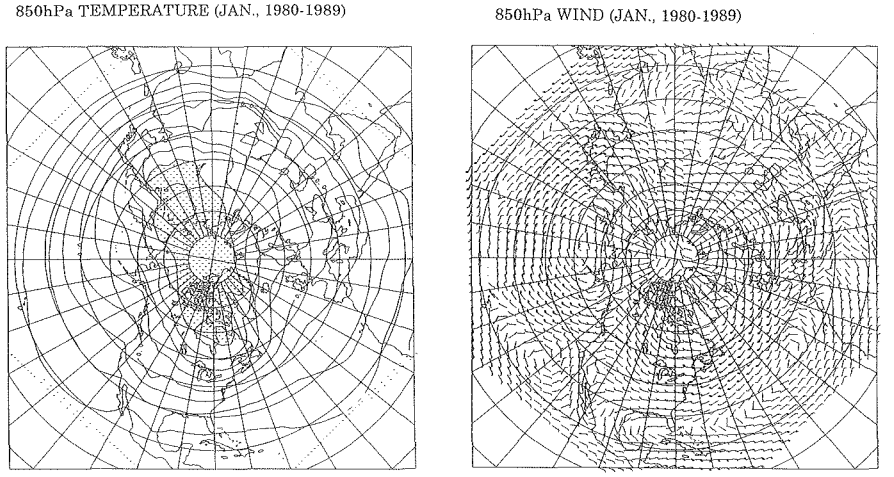

Fig. 1. Mean temperature (a) and mean wind (b) at 850 hPa in January averaged from 1980 to 1989 by the NMC data set. The interval of the isotherm is 5°C. Colder region less than −20°C is shaded.

averaged from 1980 to 1989 from the NMC data set (National Meteorological Center Grid Point Data Set). The minimum temperature region (colder than −20°C) extends southward over the east edge of the Eurasian Continent and also to the central North American Continent. Strong northerly winds blow from the north pole over these regions. This wind pattern is strongly affected by the topography. Looking at the cold region in North America, it extends from the western mountainous regions of the Mackenzie and Rocky Mountains to Greenland in the east. The meandering meridional circulation passing through the north of Alaska merges with the anticlockwise circulation from Greenland and flows southeastward. The air masses in both air streams march over the relatively flat frozen Arctic Ocean and the plateau of the Canadian Shield. Figure 2 shows the mean surface temperature in January averaged from 1951 to 1980 provided by the Atmospheric Environment Service (AES), Canada. An extremely cold region (colder than −34°C) exists over King William Island. This cold region extends toward eastern Victoria Island, the Boothia Peninsula and the northwestern shore of Hudson Bay. This cold air mass advects into southeastern Canada where anticyclogenesis frequently takes place. So, how is this cold air mass produced? Do condensed materials actually play an important role as proposed by Curry (1983, 1987)?

To obtain answers to this question, energy budget observations were car-

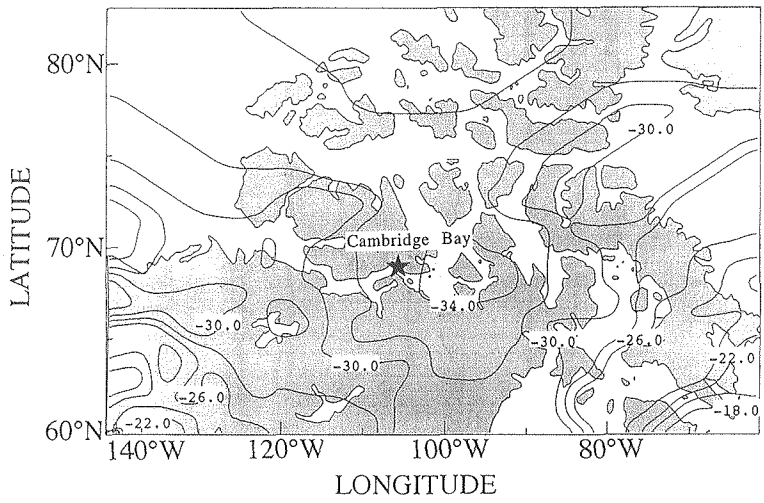

Fig. 2. Mean surface temperature of Canadian Arctic in January from 1951 to 1980 provided by Atmospheric Environment Service (AES), Canada. The interval of the isotherm is 2°C. The location of Cambridge Bay is indicated by a star.

ried out at Cambridge Bay (69°07′N, 105°03′W), N.W.T., Canada from January 14 to February 9 in the mid-winter of 1994. The location of Cambridge Bay is indicated with a star in Fig. 2. This site was selected for several reasons; (1) adjacent location to the surface temperature cold region as shown in Fig. 2, (2) meteorological technical support was available from the AES Weather Station including regular upper air soundings, (3) suitable accommodation, a good sized town (about 1,400 population in Cambridge Bay) and good transportation (several jet flights are scheduled every day from Edmonton).

2. The overall weather conditions during the observation period

Air temperature and pressure variations at the ground and 850 hPa obtained from upper air soundings at Cambridge Bay are shown in Fig. 3. The surface temperature varied between −20°C and −40°C during this period. Very cold surface temperatures appeared three times, from January 14 to 16, January 22 to 27, and February 4 to 5. Unfortunately, the first event was missed because the equipment was not completely set up. Four periods were classified according to surface temperature. They were: I, warm period from January 17 to 22; II, cold period from January 23 to 27; III, warm and disturbed period from January 28 to February 4 (clouds and blizzard were observed in this period);

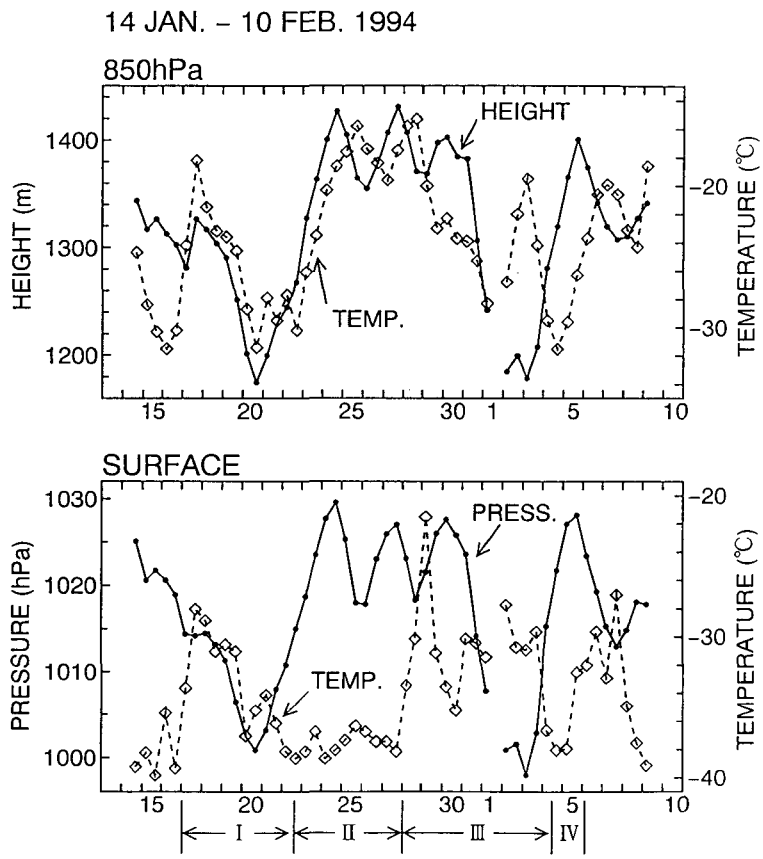

Fig. 3. Air temperature and pressure variations at the ground and 850 hPa from upper air sounding at Cambridge Bay. The solid lines indicate the pressure and the dashed lines indicate the air temperature. Four periods are classified by surface temperature as shown in the bottom.

IV, cold period from February 4 to 5. These periods are shown on the bottom of Fig. 3. Surface pressure varied between 995 hPa and 1030 hPa. Cold surface temperatures were observed from the surface trough to the ridge passage. When the observation site was under a trough, the surface temperature decreased and remained cold under the ridge. When the next trough approached, relatively warm temperatures were observed on the ground. Remarkable surface temperature warming was observed January 17, 28 and February 5. The amount of the increase was 12°C in 24 hours for January 17, 17°C in 36 hours for January 28 and 5.6°C in 12 hours for February 5. These warming trends occurred with strong winds associated with the approaching trough. At 850

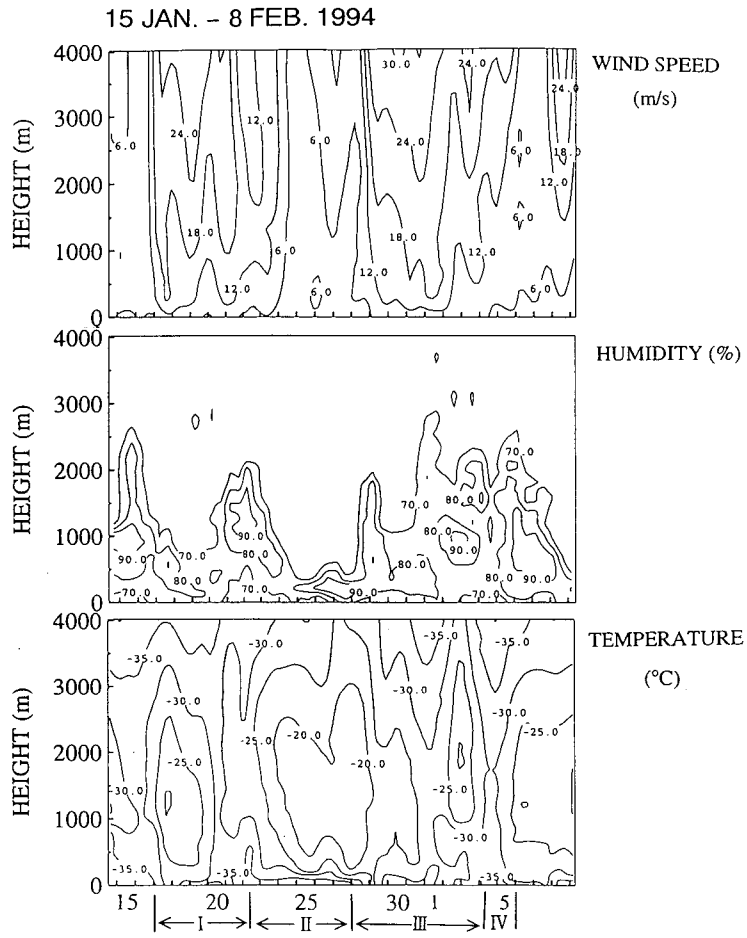

Fig. 4. Time-height cross section of wind speed, relative humidity and air temperature from upper air sounding at Cambridge Bay. The interval of the contour lines of wind speed is 6m/s, that of relative humidity is 10% and that of air temperature is 5°C. The contour lines are drawn higher than 70% in relative humidity.

hPa, the temperature varied between −16°C and −32°C and the geopotential height ranged from 1170 m to 1430 m. A distinct positive correlation can be seen between the temperature and pressure variations. Cold temperatures appeared in the trough and warm temperatures appeared in the ridge. The temperature variation seemed to have a time lag of 12 hours behind the pressure variation. These variations are consistent with previous research. The cold air advection occurred in association with the approach of the trough and

adiabatic warming due to descent of the air mass occurred in the ridge.

The time-height cross section of wind speed, relative humidity and temperature is shown in Fig. 4. During the surface cold periods (II and IV), there were very weak winds though the entire layer and a strong temperature inversion was observed near the surface. The layer was quite moist under the inversion, but warm and very dry above the inversion. This dry and warm layer was formed by adiabatic warming of descending air in the ridge. As this dry and warm layer did not disturb the radiative cooling below the inversion, its strength intensified. During the surface warm periods (I and III), although the surface temperature was relatively warm, the entire layer was colder compared with the surface cold periods (II and IV). The wind speed was stronger and the air was relatively humid through the whole layer during the surface warm periods (I and III).

In summary, cold surface periods (II and IV) began with the passage of a trough and continued until the next trough approached. The surface temperature became very cold owing to radiative cooling and a strong inversion layer was created with very high humidity. Warm and dry air existed above the inversion layer formed by the adiabatic warming of synoptic scale descent. As this layer did not disturb the radiative cooling under the layer, cooling continued in the inversion layer and the inversion intensified. As the cold core strengthened, the air mass gradually descended over the inversion and adiabatic warming occurred. A positive feed back circulation was operating to intensify the inversion. On the other hand, the warm periods (I and III) occurred during the approach of the trough. The wind became stronger, the inversion layer near the ground surface was destroyed and it became relatively warmer and drier near the ground surface, but upper levels became colder and more humid.

3. Observation instruments

Instruments were installed in the observation field of the Cambridge Bay Upper Air Station and on the 200 m Non Directional Beacon (NDB) tower about 1km away from the upper air station. Both sites were located outside of the village and human activities did not affect the observation sites. Snapshots of the sites and equipment are shown in Fig. 5. Measured parameters are listed in Table 1.

Upward and downward total radiation (0.3-2.8 μm) fluxes ($K^{\uparrow}$, $K^{\downarrow}$), near infrared (0.7-2.8 μm) fluxes ($NIR^{\uparrow}$, $NIR^{\downarrow}$), infrared radiation (4-50 μm) fluxes ($L^{\uparrow}$, $L^{\downarrow}$) and net radiation (0.3-30 μm) (Q^{*}) instruments were installed on a

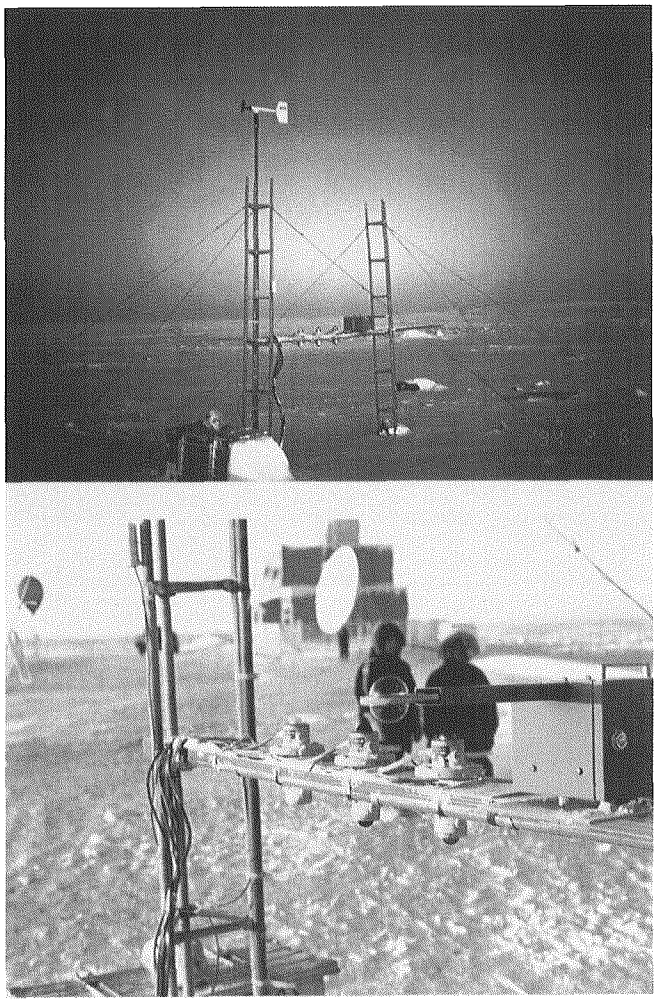

Fig. 5. Snapshots of equipment.

wooden platform 1.3 m high as shown in Fig. 5. Air temperature (T_a) was measured at 1.8 m and the ground surface temperature (T_s) was at 0.3 m before 12 : 00 LST January 26 and on the ground after 12 : 00 LST January 26. The wind was measured at 3 m at the upper air station site. The air temperature and wind speed were measured at 20 m, 40 m and 66 m by automated measuring instruments on the NDB tower from September, 1993 to April, 1994. The air temperature at 3.7 m and the temperature difference between 3.7 m and 1.25 m

Table 1. Measured parameters for the energy budget observation.

Instruments
Intensive Observation
Upper Air Station
Upward/Downward Total Flux ($K^{\uparrow}$, $K^{\downarrow}$)
(0.3-2.8 μm), $H=1.3$ m
Upward/Downward Near-IR Flux ($NIR^{\uparrow}$, $NIR^{\downarrow}$)
(0.7-2.8 μm), $H=1.3$ m
Upward/Downward Infrared Flux ($L^{\uparrow}$, $L^{\downarrow}$)
(4-50 μm), $H=1.3$ m
Net Radiation (Q^*)
(0.3-30 μm), $H=1.5$ m
Air Temperature (T_a)
$H=1.8$ m
Surface Temperature (T_s)
$H=0.3$ m (before 12 : 00 LST January 26)
Surface (after 12 : 00 LST January 26)
Wind Speed & Wid Direction
$H=3$ m
Automatic Measuring Instruments
Non Directional Beacon (NDB) Towor
Air Temperature
Wind Speed
$H=20$ m, 40 m, 66 m
Upper Air Station
Air Temperature
$H=3.7$ m
Temperature Differene
3.7 m-1.25 m

were also automatically monitored at the upper air station through the same period.

4. Results

Time variations of the air temperature at 66 m and at the surface, and their difference observed at the NDB tower are shown in Fig. 6. Energy budget elements observed at the upper air station are shown in Fig. 7. Arrows in the figure show the defrosting of the downward infrared radiation dome. Discontinuities in the records appeared in the downward infrared radiation and net infrared radiation. In the following section, the observational results will be shown classified as the cold and warm periods.

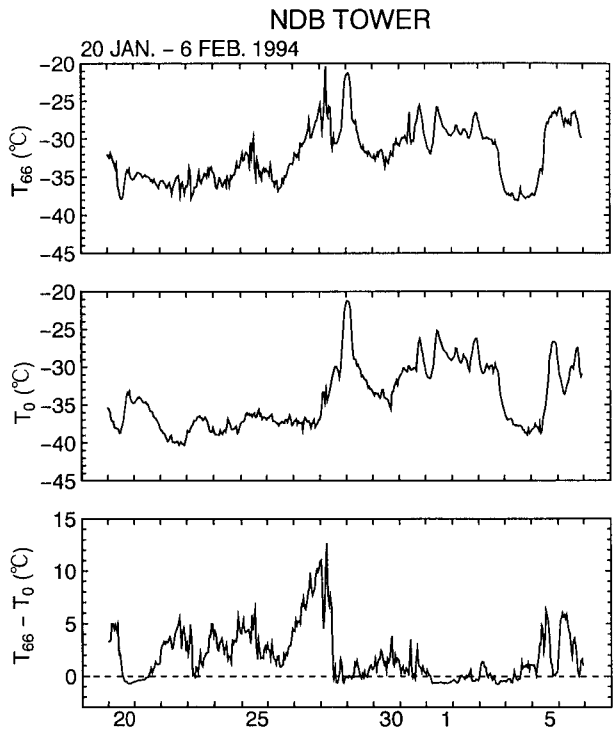

Fig. 6. Time variations of the air temperature at 66 m in height and at the surface, and their difference on the Non Directional Beacon tower.

4.1 Cold period (II)

Meteorological elements measured at the NDB tower are shown in Fig. 8 and the energy budget elements are shown in Fig. 9 for the cold period (II). The domes of the downward flux radiometers of total radiation ($K^{\downarrow}$), near infrared radiation ($NIR^{\downarrow}$) and infrared radiation ($L^{\downarrow}$) were defrosted at 14 : 30 LST on January 25 and 12 : 00 LST on January 26. Discontinuities of downward total radiation ($K^{\downarrow}$), infrared radiation ($L^{\downarrow}$) and net infrared radiation (ΔL) were recorded in Fig. 9 owing to the frosts. As the domes of net radiation (Q^*) were made of polyethylene, frosts did not form on these domes.

The air temperature (T_0) indicated an almost constant value of −37°C at 3.7 m. There was surprisingly little fluctuation. Solar insolation was so small that diurnal variations were negligible. The temperature at 66 m (T_{66}) varied between −30°C and −35°C. This fluctuation was larger than that at the surface, but it was still small. A strong temperature inversion existed during this

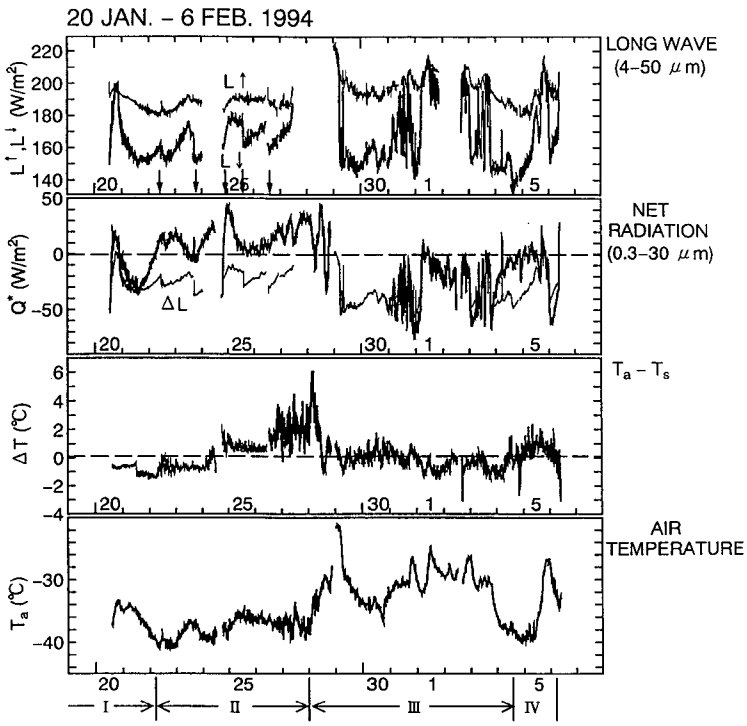

Fig. 7. Time variations of energy budget elements observed at the upper air station during the entire period. Downward and upward infrared radiation flux ($L^{\downarrow}$, $L^{\uparrow}$), net radiation (Q^*), net infrared radiation (ΔL), air temperature at 1.8 m in height (T_a) and temperature difference between 1.8 m and surface (T_a-T_s). Thick arrows in the infrared radiation show the defrosting of the downward infrared radiation dome.

period. The temperature difference (T_{66}-T_0) between the ground and 66 m in height was approximately 4°C with a maximum of 9°C. Wind speeds were very light (less than 10 m/s even at 66 m in height). The temperature difference (T_{66}-T_0) was larger during the weaker winds before 12 : 00 LST on January 25 and after 18 : 00 LST on January 26, and smaller in relatively stronger winds ($\approx$10 m/s), even though the air temperature on the ground (T_0) stayed almost constant.

From Fig. 9, the surface temperature (T_s) was about 2-3 degrees lower than the air temperature (T_a) at 1.8 m. Note that the surface temperature (T_s) was actually measured at 0.3 m before 12 : 00 LST on January 26. The upward infrared radiation was recorded at an almost steady value of about 190 W/m². This correlates nicely with the constant surface temperature. The downward

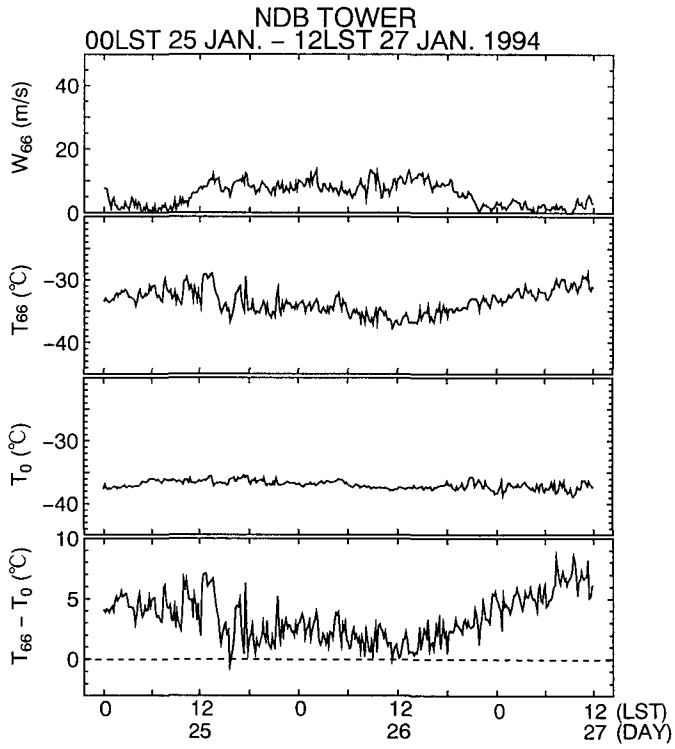

Fig. 8. Time variations of the wind speed and air temperature at 66m in height and at the surface, and their difference on the Non Directional Beacon tower during the cold period (II).

infrared radiation gradually increased but this was probably a function of the frosting on the dome. It is estimated that the downward infrared radiation kept an almost constant value of about 160 W/m². The net infrared radiation ($\Delta L = L^{\downarrow} - L^{\uparrow}$) was therefore around -30 W/m². The solar insolation is very weak during the polar winter and was less than 60 W/m² at maximum, and its contribution to the energy budget was very small. The net radiation (Q^*) indicated positive values during this period. It fluctuated between 0 W/m² and 50 W/m². Larger positive values of net radiation (Q^*) appeared before 12 : 00 LST on January 25 and after 18 : 00 LST on January 26. The variations are well correlated with the intensity of the inversion, that is, the temperature difference (T_{66}-T_0) between the ground and 66 m from the NDB tower measurements. This discussion appears later in this paper.

The vertical temperature and humidity profiles from the radiosonde obser-

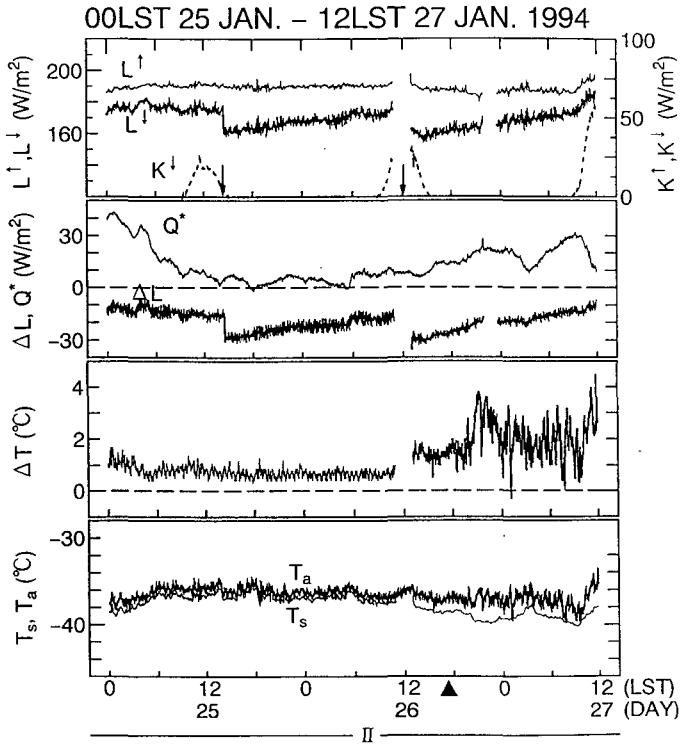

Fig. 9. Time variations of energy budget elements observed at the upper air station during the cold period (II). Downward and upward infrared radiation flux ($L^{\downarrow}$, $L^{\uparrow}$), total radiation flux($K^{\downarrow}$, $K^{\uparrow}$), net radiation (Q^*), net infrared radiation (ΔL), air temperature at 1.8 m in height (T_a) and temperature difference between 1.8 m and surface ($T_a - T_s$). A triangle in the bottom shows the time of upper air sounding in Fig. 10.

vation at 17 : 00 LST on January 26 are shown in Fig. 10. The air temperature was −37°C at the surface and −17°C at 1.1 km in height. The depth of this inversion layer was about 1.2 km and the temperature difference was approximately 20°C. The air mass was saturated between 200 m and 600 m ASL. This indicated that supercooled or cloud droplets could be produced in this layer. Relatively colder temperatures were observed at the top of the saturated layer around 600 m ASL and it was not saturated at the surface. The air mass above the inversion layer was relatively dry, as previously mentioned.

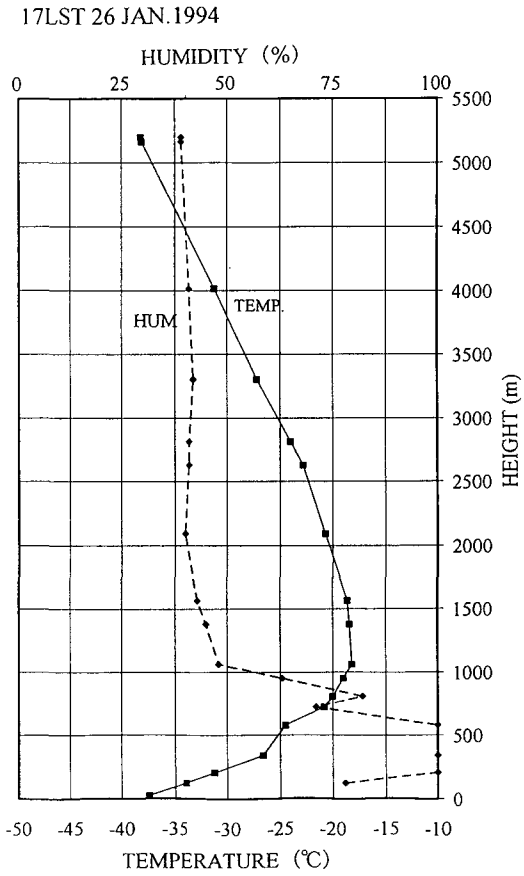

Fig. 10. Vertical temperature and humidity profiles from the radiosonde sounding at 17 : 00 LST on January 26. The solid line shows air temperature and the dashed line shows relative humidity.

4.2 *Warm period (III)*

a) Under the clouds

The results under the clouds are shown in Figs. 11 and 12. Figure 12 shows that the surface temperature (T_s) was warmer than the air temperature (T_a). This tendency can also be seen clearly in the NDB tower readings in Fig. 11. Strong winds were fairly steady at about 20 m/s. When the clouds appeared, the air temperature on the ground (T_0) was almost the same or higher than that at 66 m. The temperature difference ($T_{66}-T_0$) varied between 0°C and −0.6°C, and the temperature inversion did not appear during the cloudy conditions.

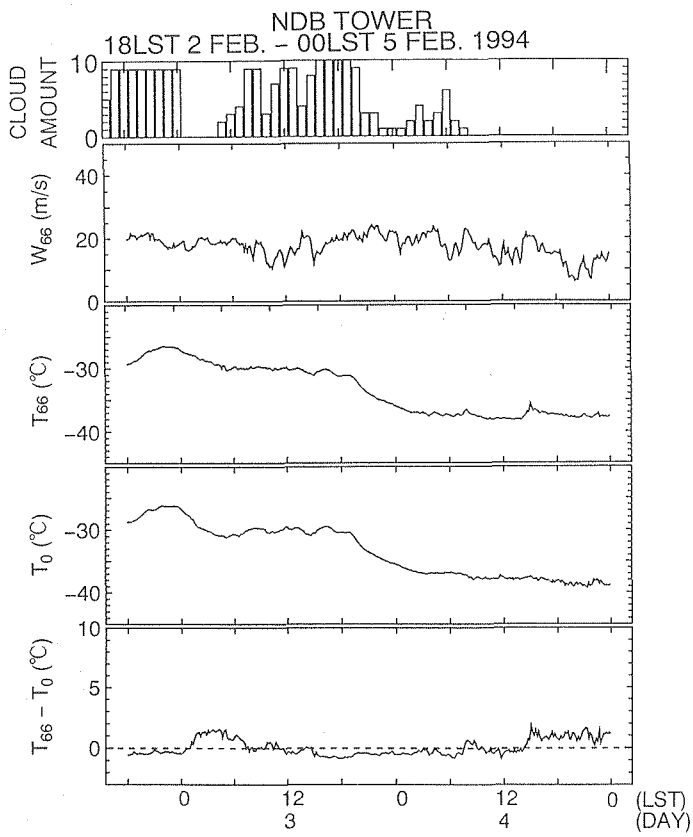

Fig. 11. Same as Fig. 8 but for under the clouds (III) and cloud amount.

The −0.6°C temperature difference between the ground and 66 m reflects the dry adiabatic lapse rate. This implies that mechanical mixing occurred near the surface owing to the strong winds in the lower layer. Therefore, the temperature differences of between 0°C and −0.6°C were quite reasonable under the cloud cover. Temperature inversions were created very quickly when the clouds disappeared.

With regards to the energy budget components, the upward long wave radiation ($L^{\uparrow}$) varies in proportion to the surface temperature and measurements showed the fluctuation to be between 180 W/m² and 210 W/m². The downward infrared radiation ($L^{\downarrow}$) fluctuated between 140 W/m² and 160 W/m² when the sky was clear and it increased to around 200 W/m² under cloudy skies. The net infrared radiation (ΔL) was, therefore, between −50 W/m² and −40

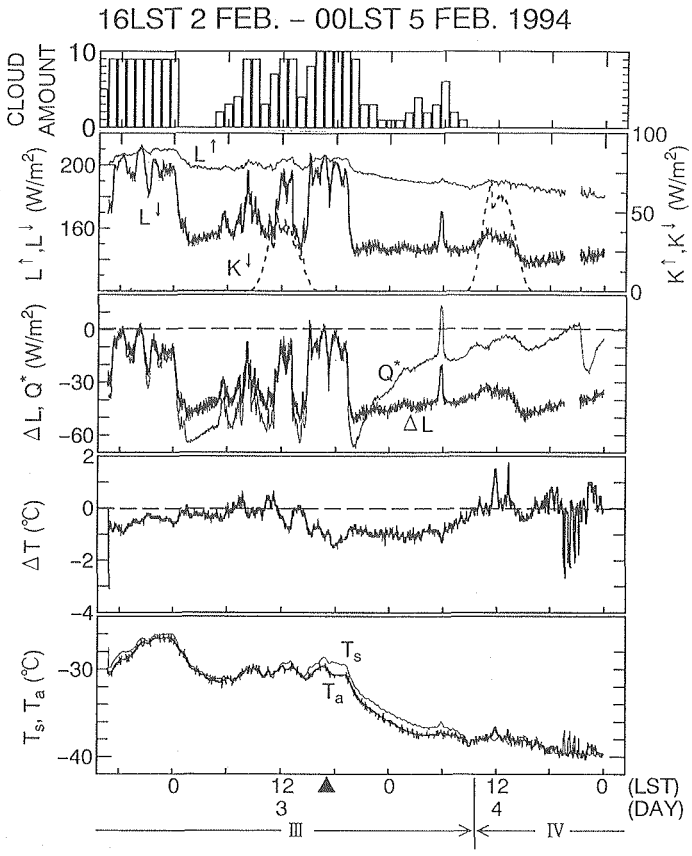

Fig. 12. Same as Fig. 9 but for under the clouds (III), cloud amount and Fig. 13.

W/m² during clear skies and between −10 W/m² and 0 W/m² under cloud. The net radiation (Q^*) indicated around −60 W/m² for the beginning of the clear period and indicated smaller values as the clear sky continued. Under the cloud, it indicated values between −10 W/m² and 0 W/m². It was almost the same amount as the net infrared radiation (ΔL) indicated.

The upper air data at 17 : 00 LST on February 3 is shown in Fig. 13. It was inferred that a cloud layer existed between 1.5 km and 2.1 km ASL. An almost isothermal layer of around −25°C was indicated within the cloud layer. A closer look shows that the temperature was a little colder at the cloud top than at the cloud base. Another isothermal layer of about −30°C was observed near the surface. Takeda et al. (1982) reported that the temperature profiles of winter Arctic stratiform clouds were isothermal in the cloud. They surmised

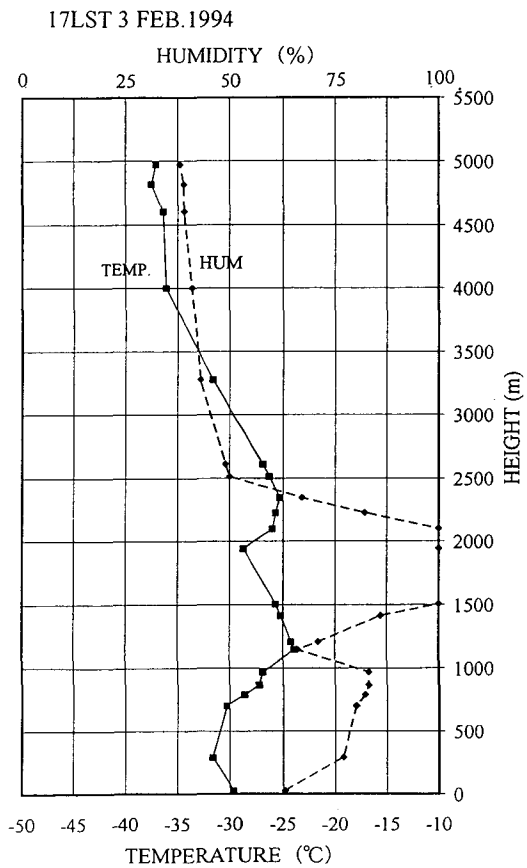

Fig. 13. Same as Fig. 10 but for February 3.

that the radiative cooling of the cloud droplets made this layer isothermal.

b) Blizzard

The case of the blizzard is shown in Figs. 14 and 15. AES hourly observations taken at the Cambridge Bay Weather Station indicated that the Blizzard started at 08 : 00 LST on January 31 and continued intermittently until 15 : 00 LST. It started again at 00 : 00 LST on February 1 and continued until 09 : 00 LST on February 2. The wind at 66 m, observed at the NDB tower, indicated over 20 m/s with a maximum of 40 m/s. The wind on the ground indicated over 10 m/s at 06 : 00 LST on February 1 and over 20 m/s at 12 : 00 LST. The temperature difference between 66 m and the ground was around −0.6°C (dry adiabatic lapse rate) owing to mixing by the strong winds.

The upward infrared radiation varied between 195 W/m^2 and 215 W/m^2

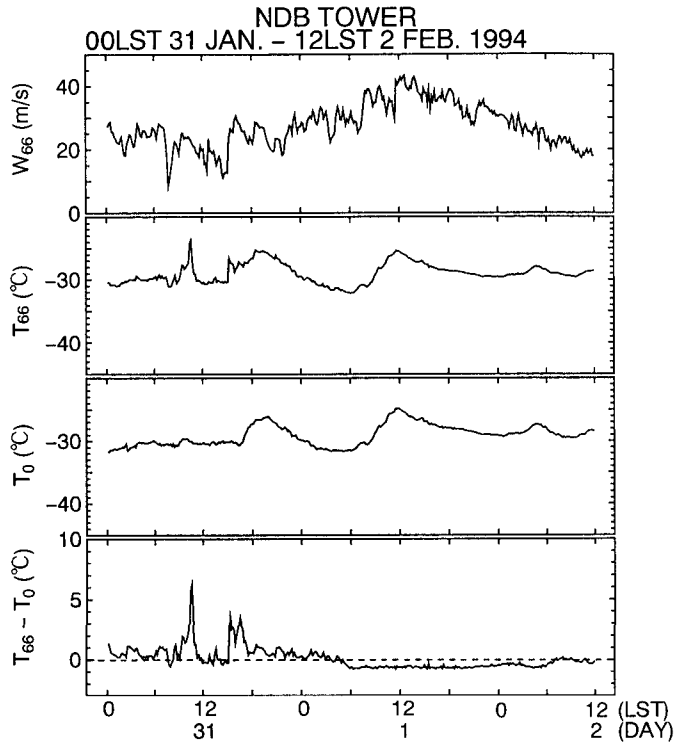

Fig. 14. Same as Fig. 8 but for during blizzard (III).

owing to the surface temperature and blowing particles underneath the radiometer. The downward infrared radiation was more than that during clear skies due to the radiation from snow particles blown up above the radiometer by the blizzard. The net infrared radiation was almost 0 W/m^2 owing to the balance of upward and downward radiative fluxes. The net radiation (Q^*) behaved almost the same as the net infrared radiation (ΔL).

The upper air sounding is shown in Fig. 16. A strong temperature inversion layer of about 8°C temperature difference was observed at 1km ASL. Under this inversion layer, the air mass was mechanically well mixed. The observed lapse rate was about 7°C/100 m in this layer. The relative humidity was less than 80% with respect to water and saturated with respect to ice. As the saturated vapor pressure with respect to ice is much smaller than that with water in the very cold temperatures below the freezing level, the relative humidity was relatively lower in this layer.

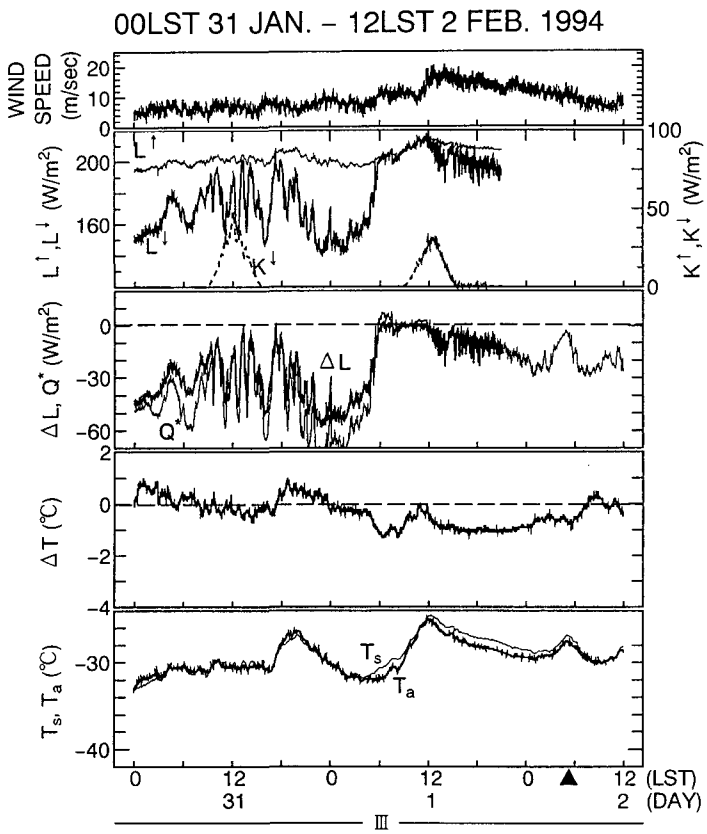

Fig. 15. Same as Fig. 9 but for during blizzard (III) and Fig. 16.

4. Discussion

The net infrared radiation (ΔL) and the net radiation (Q^*) exhibited almost the same behavior under the clouds and during the blizzard. Different behavior occurred during clear sky conditions. In these conditions, a strong inversion layer was created near the surface. The air mass in the inversion layer became very cold and water vapor would condense near the top of the inversion layer due to the entrainment of the free atmosphere. Curry (1983, 1987) simulated the air mass formation taking into account this process and concluded that this process is effective in transforming the relatively warm marine polar air mass into a cold continental polar air mass. As the upper air sounding in Fig. 10 shows, a saturated layer with respect to water was observed near the top of the

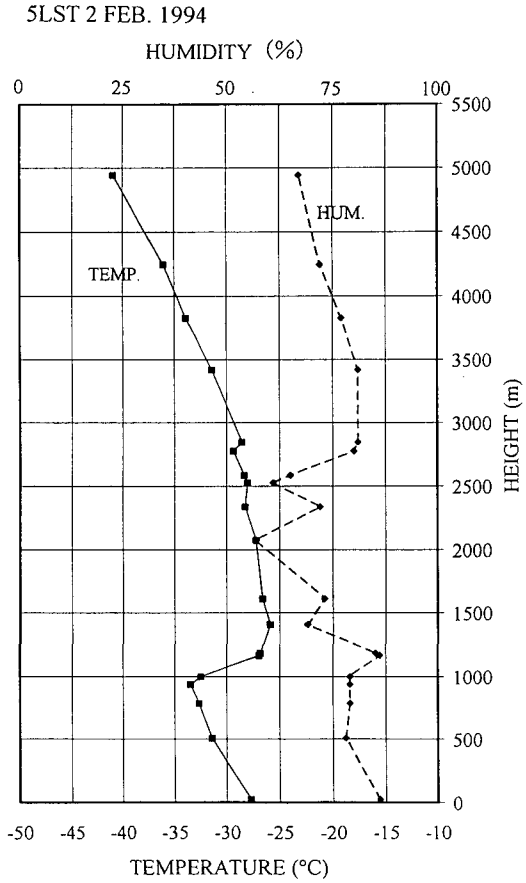

Fig. 16. Same as Fig. 10 but for 05 : 00 LST February 2.

inversion layer. Net radiation (Q^*) would be affected by the radiation from these water droplets. To examine this scenario, Figure 17 shows the relationships between the net radiation amounts (ΔL, Q^*) and the temperature difference between 66 m and the surface ($T_{66}-T_0$), as the indicator of the inversion strength. The net infrared radiation (ΔL) always indicated negative values even though it indicated smaller values during the stronger inversion. Although frosting on the dome of the radiometer may disturb the examination of this relationship, it is obvious that radiative cooling occurred at the surface even after the strong inversion appeared. Regarding the net radiation (Q^*), Figure 17(b) shows that positive values were dominant during the strong inversion. There is evidence that the net radiation amount was proportional to the inver-

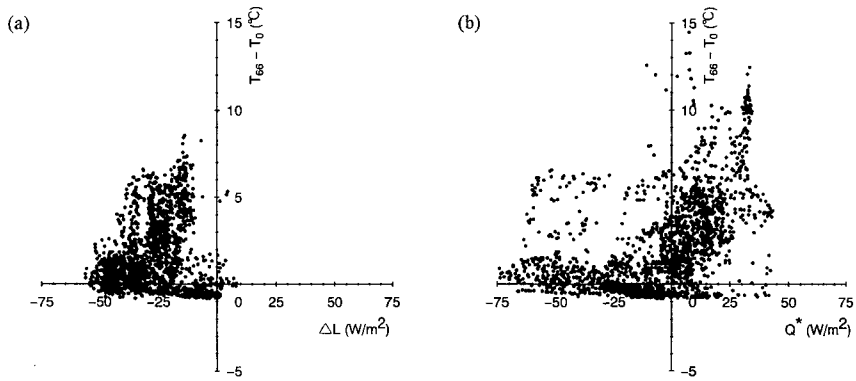

Fig. 17. Relationships between net infrared radiation flux (ΔL) and temperature difference between 66m and the ground ($T_{66}-T_0$) (a) and between net radiation flux (Q^*) and temperature difference ($T_{66}-T_0$) (b).

sion strength. The condensed matter might be small supercooled cloud droplets of several microns in diameter. The radiation from these small supercooled cloud droplets and drizzle may be sensed by the net radiation instrument (Q^*) but may not be sensed by the infrared radiometer (ΔL). The measurable wave lengths for the net radiation radiometer (Q^*) are from 0.3 to 30 μm and that for the infrared radiometer (ΔL) are from 4 to 50 μm. This difference might affect the detectability of the radiation from the condensed materials.

Cold air was produced by radiative cooling and accumulated near the surface under clear skies. When the trough approached and wind speed increased, it would mix up to the middle troposphere and be transported downstream to contribute to anticyclogenesis. Anticyclogenesis frequently took place in southeastern Canada. And further, when negative vorticity advected into the upper level of this region, anticyclogenesis would be enhanced.

5. Concluding remarks

To examine the formation processes of cold air masses, energy budget observations were carried out at Cambridge Bay (69°07′N, 105°03′W), N.W.T., Canada, from January 14 to February 9 in 1994. A series of cold air mass formations under clear sky, under cloud and during blizzard conditions were observed in this period. Typical energy amounts in the various weather conditions were summarized in Table 2. The cold air mass was produced near the surface as the ridge passed. When a trough approached, the wind became stronger, cold air was mixed upward and transported downstream and may have

Table 2. Summary of the typical energy amounts in the various weather conditions.

Energy Budget Observation
Ridge
Infrared Flux (4~50 μm)
$L^{\downarrow} \approx 160$ W/m^2
$L^{\uparrow} \approx 190$ W/m^2
$\Delta L \approx -30$ W/m^2
Net Radiation (0.3~30 μm)
$Q^* \approx 0 \sim 30$ W/m$^2 \propto T_{66} - T_0$
(Condensed Matter in the Inversion Layer Expected)
Temperature Difference
$T_{66} - T_0 \approx 5 \sim 10$ °C
Trough
Under Cloud
Infrared Flux (4~50 μm)
$L^{\downarrow} \approx 190$ W/m^2
$L^{\uparrow} \approx 200$ W/m^2
$\Delta L \approx -10$ W/m^2
Net Radiation (0.3~30 μm)
$Q^* \approx \Delta L \approx -10$ W/m^2
Temperature Difference
$T_{66} - T_0 \approx 0 \sim -0.6$ °C
Blizzard
Infrared Flux (4~50 μm)
$L^{\downarrow} \approx 200 \sim 210$ W/m^2
$L^{\uparrow} \approx 210$ W/m^2
$\Delta L \approx 0 \sim -10$ W/m^2
Net Radiation (0.3~30 μm)
$Q^* \approx \Delta L \approx 0 \sim -10$ W/m^2
Temperapure Difference
$T_{66} - T_0 \approx -0.6$ °C (Dry-Adiabatic Lapse Rate)

contributed to anticyclogenesis.

Furthermore, from a boundary layer meteorology point of view, the air temperature on the ground indicated almost the same temperature of −37°C for several days in the cold period. It can be inferred that the heat fluxes were in balance in the boundary layer during this condition. Surface radiative cooling was balanced with the amount of eddy transport in the boundary layer and the conductive transport into the ground. To examine further processes, more

detailed analyses are needed. This will be discussed in a follow-up paper on boundary layer meteorology.

Acknowledgments

The authors would like to express their thanks to the crew members of the Cambridge Bay Weather Station of Atmospheric Environment Service (AES), Canada, especially Rick Gillis, manager of the weather station and his family for their support and encouragement of our observations in Cambridge Bay, and to Ken Marianix, Transport Canada for support of the Non Directional Beacon tower. They also wish to express their thanks to Mike Crowe, Atmospheric Environment Service (AES), Canada, for carefully proof reading the manuscript.

References

Bodurtha, F.T., Jr., 1952. An investigation of anticyclogenesis in Alaska. J. Meteor., **9**, 118-125.

Bowling, S.A, T. Ohtake and C.S. Benson, 1968. Winter pressure systems and ice fog in Fairbanks, Alaska. J. Appl. Met., **7**, 961-968.

Colucci, S.J. and J.C. Davenport, 1987. Rapid surface anticyclogenesis: Synoptic climatology and attendant large-scale circulation changes. Mon. Wea. Rev., **115**, 822-836.

Curry, J., 1983. On the formation of continental polar air. J. Atmos. Sci., **40**, 2278-2292.

Curry, J., 1987. The contribution of radiative cooling to the formation of cold-core anticyclones. J. Atmos. Sci., **44**, 2575-2592.

Dallavalle, J.P. and L.F. Bosart, 1975. A synoptic investigation of anticyclogenesis accompanying North American polar air outbreaks. Mon. Wea. Rev., **103**, 941-957.

King, M.L., P.J. Smith and A.R. Lupo, 1995. A diagnosis of the development of a winter anticyclone over North America. Mon. Wea. Rev., **123**, 2273-2284.

Konrad, C.E., II, 1996. Relationships between the intensity of cold-air outbreaks and the evolution of synoptic and planetary-scale features over North America. Mon. Wea. Rev., **124**, 1067-1083.

Konrad, C.E. II and S.J. Colucci, 1989. An examination of extreme cold air outbreaks over eastern North America. Mon. Wea. Rev., **117**, 2687-2700.

Nakamura, N. and A.H. Oort, 1988. Atmospheric heat budgets of the polar regions. J. Geophys. Res., **93**, 9510-9524.

Oort, A.H., 1974. Year-to-year variations in the energy balance of the Arctic atmosphere. J. Geophys. Res., **79**, 1253-1260.

Takeda, T., Y. Fujiyoshi and K. Kikuchi, 1982. Observation of wintertime clouds and precipitation in the Arctic Canada (POLEX-North). Part I.: Characteristic features of clouds and precipitation. J. Meteor. Soc. Japan., **60**, 1203-1214.

Tan, Y.-C. and J.A. Curry, 1993. A diagnostic study of the evolution of an intense North American anticyclone during winter 1989. Mon. Wea. Rev., **121**, 961-975.

Tanaka, H.L. and M.F. Milkovich, 1990. A heat budget analysis of the polar troposphere in and around Alaska during the abnormal winter of 1988/89. Mon. Wea. Rev., **118**, 1628-1639.